HYDROLOGICAL PROCESSES
Hydrol. Process. **19**, 77–94 (2005)
Published online in Wiley InterScience (www.interscience.wiley.com). DOI: 10.1002/hyp.5775

Distribution of soil carbon stocks in Canada's forests and wetlands simulated based on drainage class, topography and remotely sensed vegetation parameters

Weimin Ju* and Jing M. Chen
Department of Geography, University of Toronto, Toronto, Ontario, Canada

Abstract:

A quasi-three-dimensional hydrological model was developed and integrated into the integrated terrestrial ecosystem carbon-budget model (InTEC V3·0) to improve the estimation of the carbon (C) dynamics in Canadian forests and wetlands. Climate, soil, digital elevation map, and drainage class data, in conjunction with remotely sensed vegetation parameters, including leaf area index, land cover type, and stand age, are used to drive the model. Soil is divided into three layers, for which temperature and moisture dynamics are simulated. Individual 1 km × 1 km pixels are hydrologically linked with neighbouring pixels through subsurface saturated base-flow, which is simulated using a TOPMODEL-based scheme. Soil C and nitrogen (N) dynamics are simulated using the soil submodel of CENTURY suitably modified for forests and wetlands. The interannual variation in net primary productivity is iteratively computed after integrating the effects of N, climate, stand age and atmospheric CO_2 concentration on productivity. Compared with data in the Soil Landscape of Canada, the newly updated InTEC V3·0 can capture 66·6% of spatial variations in soil C and effectively alleviate soil C underestimation in wetland areas from its predecessor (InTEC V2·0) by considering the lateral water flow and the water table variation. Copyright © 2005 John Wiley & Sons, Ltd.

KEY WORDS soil carbon; forest carbon; wetland; drainage class; topography; remote sensing

INTRODUCTION

The global carbon (C) cycle is of interest in climate change studies. Recently, a variety of terrestrial ecosystem models have been developed to simulate C, nutrient, energy and water cycles, as well as the interactions between vegetation and climate at different spatial and temporal scales. They embrace terrestrial biogeochemistry (Running and Gower, 1991; Potter *et al*., 1993; Parton *et al*., 1993; Friend *et al*., 1997; Potter, 1997), global and regional vegetation biogeography (Neilson and Marks, 1994; Neilson, 1995; Haxeltine and Prentice, 1996; Kucharik *et al*., 2000), and land–atmosphere exchange processes (Dickson *et al*., 1986; Sellers *et al*., 1986, 1996). From the improved estimation of the global C budget, it is widely recognized that the overall land surface is acting as a C sink (Potter and Klooster, 1998; Houghton, 1999, Schimel *et al*., 2001; Gurney *et al*., 2002). However, the detailed spatial distribution of terrestrial C sources and sinks is still not yet clear, and different models produce inconsistent results.

Accurate atmospheric inverse models with dense atmospheric CO_2 concentration measurements would be an ideal way to partition the C sources and sinks spatially. However, they are not yet practical, owing to data limitations and the complex interactions among C, nitrogen (N), water cycles and the atmosphere. Use of remote-sensing data may be currently a practical solution to obtaining the spatial information needed on terrestrial C sources and sinks. Chen *et al*. (2003) developed a spatially distributed integrated terrestrial ecosystem carbon-budget model (InTEC V2·0) on the basis of a spatially aggregated model (InTEC V1·0;

* Correspondence to: Weimin Ju, Department of Geography, University of Toronto, 100 St George St., Rm 5047, Toronto, Ontario M5S 3G3, Canada. E-mail: juw@geog.utoronto.ca

Received 13 May 2003
Accepted 01 March 2004

Chen *et al*., 2000a) to simulate annual C balance of Canada's forests at 1 km spatial resolution. Similar to its predecessor, InTEC V2·0 integrates the effects of various factors on C dynamics, including climate, CO_2 concentration in the atmosphere, N availability, and forest stand age. Validated against soil C stock data available in the Soil Landscape of Canada (SLC) database and CO_2 flux tower data observed at some sites, the InTEC V2·0 proved the possibility of simulating long-term spatio-temporal C dynamics at large scales with certain degrees of accuracy, thanks to the use of a variety of key spatial data sets, including those derived from remote sensing (land cover, leaf area index (LAI), recent forest stand age).

Soil C is one of the key variables for estimating terrestrial C dynamics, since it is a major determinant of the amount of CO_2 released to the atmosphere through decomposition of organic matter in soils. Improved knowledge of the amount and spatial distribution of the C stock in soils is crucial to estimating changes in the terrestrial C dynamics (Bhatti *et al*., 2002). Soil C storage is determined by the balance of C input from plant primary production and C release through decomposition. Disturbance, land-use history, climate, soil texture, topography, and hydrology are the primary variables that influence both production and decomposition processes and, therefore, the total amount of soil C stocks. Soil moisture controls the amount of C assimilated by vegetation photosynthesis and C decomposed in soils and, therefore, is a key controller of soil C stocks (Parton *et al*., 1993; Trumbore and Harden, 1997). Accurate description of the hydrological cycle is, therefore, necessary for reliable estimates of the soil C stock and its variation.

Wetlands, presently covering 127×10^6 ha, or 14% of the landscape of Canada, are ecologically different from other ecosystems and play an important role in the terrestrial C cycle (Frolking *et al*., 1998). In spite of their low primary productivity, these ecosystems have been continuously accumulating soil C with an average of 0·02 to 0·03 kg m^{-2} $year^{-1}$ over the past 5000 to 10 000 years (Tolonen *et al*., 1992; Gorham 1995; Rapalee *et al*., 1998) because of their very slow decomposition rates of soil organic matter. The decomposition is slow due to several factors, including the resistance of litters to decomposition, the anaerobic conditions within the saturated peat profile, and the generally low temperatures of peat due to the large heat capacities and the low thermal conductivity of moss cover (Roulet *et al*., 1997; Frolking *et al*., 2002). C stocks in wetlands are generally 5 to 50 times larger than those in upland ecosystems (Rapalee *et al*., 1998), with most stored in old and deep organic C layers (Trumbore and Harden, 1997). The strong dependence of decomposition on soil moisture and temperature makes the soil C accumulation rate in northern wetlands sensitive to disturbance and climate change. These regions have experienced significant increases in temperature in the past 100 years, and could become much warmer and even possibly drier in the future (Gough and Wolfe, 2001). These possible climate changes are expected to cause considerable changes in hydrology and a possible shift of C sinks into C sources in these regions. Similar to other ecosystem models for large-scale applications, InTEC V2·0 had hydrological processes that were simplified to vertical fluxes only and a parameterization scheme that was the same for both wetland and upland ecosystems. These simplifications inevitably introduced errors in the estimates of the C stock and its heterogeneity.

The main objectives of this paper include: (1) to introduce the pixel-based InTEC V3·0, with the main focus on the description of its newly developed hydrological submodel; and (2) to compare estimates of the average soil C in individual SLC soil polygons from two versions of the InTEC model with those in the SLC database, to demonstrate the model improvements and to identify remaining issues.

MODEL DESCRIPTION

The InTEC model combines the CENTURY model for soil C and nutrient dynamics (Parton *et al*., 1987, 1993), and Farquahar's leaf biochemical model for canopy-level annual photosynthesis (Farquhar *et al*., 1980; Chen *et al*., 1999) implemented using a temporal and spatial scaling scheme (Liu *et al*., 1999; Chen *et al*., 2000a). A detailed description about this model can be found in Chen *et al*. (2000a, 2003). Here, the major characteristics of this model are described. The historical annual net primary productivity (NPP) in the last century is progressively calculated with the consideration of the integrated effects of major controlling factors, such as climate variability, CO_2 concentration, N availability (deposited, fixed and mineralized N), and stand age (Chen *et al*., 2000a). The annual NPP value in 1994, estimated at a daily time step using the Boreal Ecosystems Productivity Simulator (BEPS; Liu *et al*., 2002), is used as a base marker for the retrospective estimation of the initial NPP value in 1901 in each 1 km $\times$ 1 km pixel. The land-cover map derived from remote sensing (Cihlar *et al*., 1998) is used to assign coefficients allocating NPP into four vegetation biomass C pools: leaf, wood, fine root, and coarse root, and to determine litter quality. The modified soil submodel of CENTURY (Parton *et al*., 1987, 1993) was incorporated in the model to simulate soil C and N dynamics. The major modifications to the original CENTURY model include: (1) in addition to foliage and fine root pools, a woody litter pool is included; (2) the soil temperature effect on decomposition is quantified using a modified Arrhenius-type equation (Lloyd and Taylor, 1994; Chen *et al*., 2000b); (3) the modifier for the effect of soil moisture on decomposition is a function of percentage water-filled pore space (Friend *et al*., 1997); (4) the rate of N fixation is a combined function of temperature, precipitation, and the size of microbial pool (Chen *et al*. 2000b); (5) the N deposition rate is spatially and temporally interpolated based on measured N deposition rates and historical greenhouse gas concentration values (Chen *et al*., 2003).

Soil hydrological submodel

A variety of algorithms have been used in biosphere and biogeochemistry models to capture the spatial and temporal variations of soil moisture, varying from one-layer, linear drying bucket models (Hybird 3·0: Friend *et al*., 1997; TEM: Raich *et al*., 1991; McGuire *et al*., 1992) to non-linear drying, multilayer models (BIOME3: Haxeltine and Prentice, 1996; CENTURY: Parton *et al*., 1987, 1993; IBIS: Kucharik *et al*., 2000; MAPSS: Neilson, 1995; NASA–CASA: Potter *et al*., 1993, 2001; Potter, 1997, 1999; SiB: Sellers *et al*., 1986, 1996). However, most of these models, including InTEC V2·0, do not consider the horizontal redistribution of soil water. This is sometimes questionable, especially in complex terrains where soil moisture is spatially heterogeneous. To remove the weakness of InTEC V2·0 in hydrological cycle simulations, a hydrological submodel was developed to provide more realistic, yet, still simple calculations of soil water and temperature dynamics for evaluating the impacts of environmental conditions on NPP and soil C decomposition.

Figure 1 schematically illustrates processes described in this quasi-three-dimensional model. The soil profile is treated as a series of three layers. The depths of these layers can vary spatially. The bottom positions of the topmost layer and lowest layer were compiled from the SLC database. The lower boundary of the middle layer is assigned a constant of 0·35 m, since most C with high decomposition rates is located above this depth (Trumbore and Harden, 1997). All hydraulic parameters except saturated hydraulic conductivity are assumed to be vertically uniform in the three soil layers. The saturated hydraulic conductivity is assumed to decline exponentially with depth from the surface (Beven, 1997). This decline rate is given a global constant, since there is still no practical method to estimate this parameter. At any time step, the model partitions precipitation into rainfall and snow according to air temperature. The interception of rainfall and snow is simply estimated as a function of LAI (Abramopoulos *et al*., 1988). The throughfall plus snowmelt can saturate soil or produce surface runoff, which depends on the water content of the topmost soil layer and the amount of available water input. Transpiration extracts water from all soil layers. However, soil evaporation is restricted to the topmost layer. Available soil moisture first feeds evaporation and transpiration, and the remainder wets the soil or percolates to the lower soil layers. In the topmost and middle layers, there is only vertical soil water transport. In the lowest layer, individual pixels are hydrologically linked with neighbouring pixels using a quasi-three-dimensional saturated subsurface water transport scheme (Wigmosta *et al*., 1994).

The decomposition rates of various C pools are modified by soil moisture and temperature in different soil layers (Potter, 1997). The temperature and moisture in the topmost soil layer control the decomposition rates of surface foliage litter and surface microbial C pools. The decomposition of other soil C pools is influenced by a weighted average of combined modifiers for the effects of soil moisture and temperature on decomposition in the middle and lowest layers. The weight of each layer is given based on the vertical distribution of active root biomass (Jackson *et al*., 1996) and drainage class at this location. If the drainage

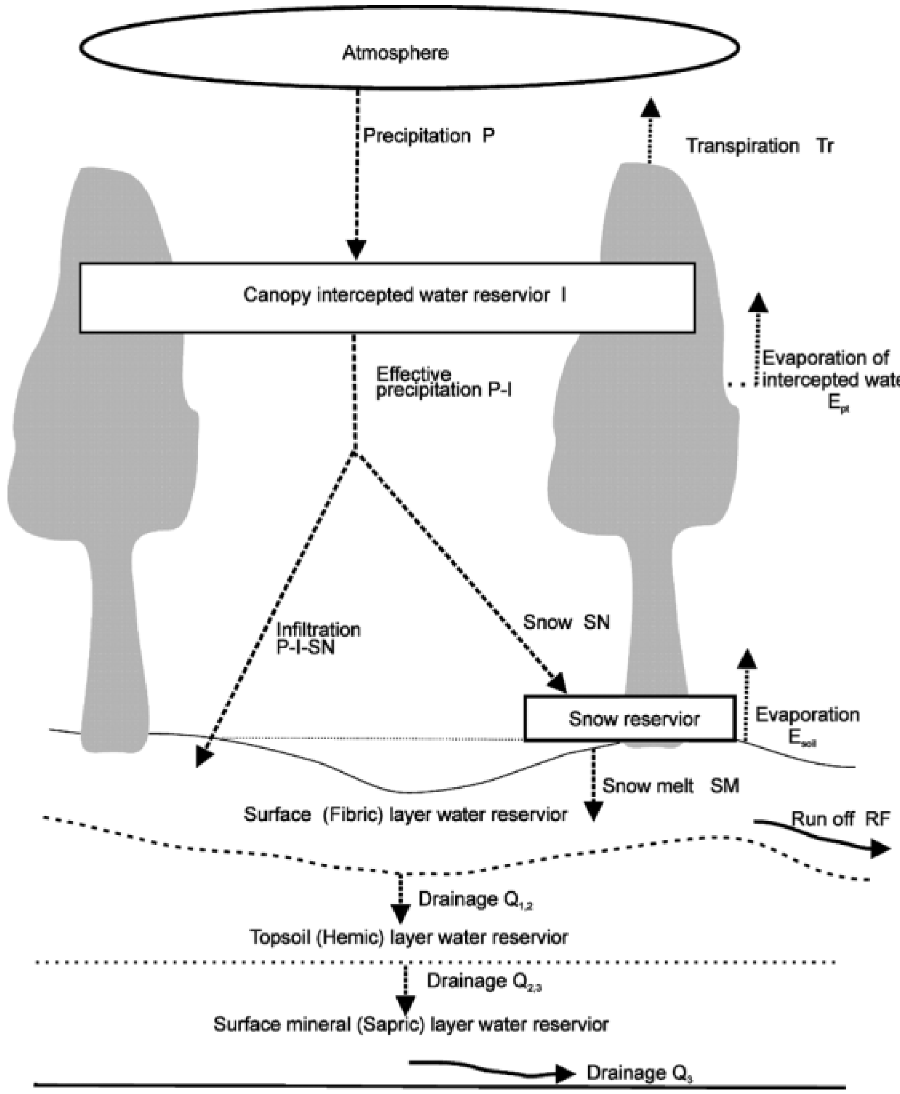

Figure 1. Structure of the hydrological submodel. This model uses a set of equations with climate, vegetation, soil and topography data to simulate soil temperature and moisture dynamics. The output from this model is used to quantify the combined abiotic effect on decomposition of soil C and NPP

condition is poor, then the temperature and moisture in the lower layer will be given a high weight affecting the decomposition process. It was found that, in poorly drained boreal areas, most soil organic C accumulates deeply and has very slow decomposition rates (Trumbore and Harden, 1997; Rapalee *et al*., 1998).

Soil water balance and redistribution

The water balance in each soil layer is calculated as the difference between the net input to and output of water from this layer, i.e.

$$\frac{\partial \theta_1}{\partial t} = \frac{1}{d_1}(P - I - \mathrm{SN} + \mathrm{SM} - T_{\mathrm{r},1} - E_{\mathrm{s}} - \mathrm{RF} - Q_{1,2}) \tag{1a}$$

$$\frac{\partial \theta_2}{\partial t} = \frac{1}{d_2}(Q_{1,2} - T_{r,2} - Q_{2,3}) \tag{1b}$$

$$\frac{\partial \theta_3}{\partial t} = \frac{1}{d_3}(Q_{2,3} - T_{r,3} - Q_3) \tag{1c}$$

where θ_i (m^3 m^{-3}) is the volumetric soil water content of the ith soil layer, d_i (m) is the thickness of the ith soil layer, P (m day^{-1}) is the total precipitation, I (m day^{-1}) is the precipitation intercepted by a canopy, SN (m day^{-1}) is the precipitation as snowfall, SM (m day^{-1}) is the melt from the snowpack, $T_{r,i}$ (m day^{-1}) is the transpiration uptake from the ith layer, E_s (m day^{-1}) is the evaporation from the topmost soil layer, RF is the surface runoff, estimated following Neilson (1995) and Arnold and Williams (1995), $Q_{i,i+1}$ (m day^{-1}) is the vertical exchange of soil water between the ith and the $(i+1)$th layer, calculated following Sellers *et al.* (1996), and Q_3 is the saturated subsurface flow and calculated as follows:

$$Q_3 = \frac{Q_{\mathrm{out}_j} - Q_{\mathrm{in}_j}}{A_j} \tag{2}$$

where Q_{out_j} and Q_{in_j} are the saturated base flows out and into pixel j respectively, and A_j is the pixel area (currently 1 km^2).

Each pixel can horizontally exchange soil water with its eight neighbouring pixels via saturated base flow. With the assumption that local slopes approximately represent local hydraulic gradients, the rate of saturated subsurface flow at time t from the jth pixel to its downslope neighbours is computed as (Wigmosta *et al.*, 1994)

$$q(t)_{j,k} = \begin{cases} T(t)_j w_{j,k} \dfrac{e_j - e_k}{d_{j,k}} & \text{if } e_j > e_k \\ 0 & \text{else} \end{cases} \tag{3}$$

where $q(t)_{j,k}$ (m^3 day^{-1}) is the flow rate from pixel j to pixel k, e_j and e_k (m) are the elevations of pixels j and k respectively, $w_{j,k}$ (m) is the width of flow from j to k, $d_{j,k}$ (m) is the distance between the centre of pixel j and pixel k, and $T(t)_j$ (m day^{-1}) is the transmissivity of soil water at pixel j and is estimated following a TOPMODEL approximation that saturated hydraulic conductivities for some soils decrease exponentially with soil depth (Sivapalan *et al.*, 1987; Wigmosta *et al.*, 1994).

It is a challenge to estimate the redistribution of soil water at a monthly time step. Based on the soil depth and porosity values compiled from the SLC database, it was found that the thickness of water in the whole soil profile is generally less than 2·0 m and much smaller than the potential of the monthly vertical movement of soil water (Campbell and Norman, 1998). The potential movement of water could exceed the available storage capacity of the soil layer at any time within a month (Neilson, 1995). To avoid this problem, and to limit the computation time, the infiltration and vertical percolation are allowed to occur at 5 day intervals with the following controls imposed. First, downward percolation is estimated as the lesser of the calculated potential flux from the upper layer and the saturation deficit of the lower layer. Second, the upward movement can, at its maximum level, recharge the upper layer above the saturated layer to the field capacity.

Computation of evapotranspiration

Evapotranspiration is calculated as the sum of transpiration of vegetation T_r, evaporation from soil E_{soil} and from the intercepted precipitation by vegetation E_{pt}, i.e.

$$\mathrm{ET} = E_{\mathrm{soil}} + E_{\mathrm{pt}} + T_r \tag{4}$$

Surface net radiation R_n is approximately partitioned between the canopy R_n^{veg} and the ground surface R_n^{soil} based on a Beer-like extinction law, i.e.

$$R_n^{\mathrm{veg}} = (1 - e^{-k\Omega \mathrm{LAI}})R_n \tag{5}$$

Table I. Parameters used in the hydrological submodel for different forest types

Parameters	Conifer	Deciduous	Mixed forest	Open land
Albedo[a]				
Winter	0·14	0·2	0·18	0·18
Spring	0·14	0·13	0·20	0·20
Summer	0·16	0·17	0·28	0·28
Autumn	0·12	0·13	0·22	0·22
Maximum LAI_{max}[a,b]	6·0	6·0	4·0	4·0
Minimum stomatal resistance r_{min} (s m^{-1})[c]	100	100	50	50
Clumping index Ω[d]	0·5	0·7	0·6	0·6
Depth coefficient of root distribution β[e]	0·943	0·943	0·914	0·914
Lower temperature limit for respiration (K)[f]	273·0	273·0	273·0	273·0
Upper temperature limit for respiration (K)[f]	318·0	318·0	318·0	318·0

[a] Stieglitz *et al.* (1997).
[b] Chen *et al.* (2002).
[c] Kergoat (1998), Saugier *et al.* (1997).
[d] Liu *et al.* (1997).
[e] Jackson *et al.* (1996).
[f] Sellers *et al.* (1986), Zierl (2001).

where k is the extinction coefficient of solar radiation and Ω is the clumping index, which depends on land cover type (Table I).

The surface net radiation consists of three components, i.e.

$$R_n = (1-\alpha)R_s \downarrow + L_a \downarrow - L_e \uparrow \tag{6}$$

where α is the albedo of canopy, which is a pre-described constant for each of major land cover types (Table I), $R_s \downarrow$ is the downward shortwave solar irradiance, and $L_a \downarrow$ and $L_e \uparrow$ represent the incoming and outgoing longwave irradiances from the atmosphere and the ground surface respectively. The incoming and outgoing irradiance are calculated from the well-known Stefan–Boltzmann law. The emissivity of the ground surface is estimated using the normalized difference vegetation index (NDVI; Griend, 1993). The emissivity of the atmosphere ε_a was parameterized following Satterlund (1979).

The canopy available energy is first used to evaporate intercepted precipitation at a potential rate. The remaining energy is then used for transpiration from the dry canopy (Kergoat, 1998). The actual transpiration rate from the dry canopy depends on the weather-controlled potential transpiration T_p and the soil moisture modifier. The value of T_p is calculated using Penman–Monteith equation with the consideration of the effects of radiation, temperature and the air water vapour pressure deficit on canopy resistance:

$$T_p = \frac{\Delta R_n^{veg} + \dfrac{\rho C_p}{r_a} d}{L\left[\Delta + \gamma\left(1 + \dfrac{r_c}{r_a}\right)\right]}(\tau_{day} - \tau_{int}) \tag{7}$$

where τ_{day} and τ_{int} are, respectively, the total day length and the fraction of day length consumed by intercepted rainfall or snowfall, Δ is the slope of the saturated vapour pressure against temperature, d is the air water vapour saturation deficit, γ is the psychrometric constant, ρ is the air density, C_p is the specific heat of air, L is the latent heat of water vaporization, r_a is the canopy aerodynamic resistance, and r_c is the bulk resistance of the canopy, computed as

$$r_c = \frac{r_{st}}{\langle LAI \rangle} \tag{8}$$

where $\langle \text{LAI} \rangle$ is the effective LAI and is computed as

$$\langle \text{LAI} \rangle = \text{LAI}_{\text{sun}} + (\text{LAI} - \text{LAI}_{\text{sun}})\frac{S_{\text{shade}}}{S_{\text{sun}}} \tag{9}$$

where LAI_{sun} is the sunlit LAI, S_{sun} is the daily mean sunlit leaf irradiance and S_{shade} is the daily mean shaded leaf irradiance. The partition of sunlit and shaded leaves and the calculation of irradiance on these two types of leaf follows Chen *et al*. (1999).

The bulk stomatal resistance r_{st} is described in the form of a minimal resistance $r_{\text{st,min}}$ (Table I) multiplied by the product of independent stress functions, i.e.

$$r_{\text{st}} = r_{\text{st,min}} F_1(S_{\text{sun}}) F_2(T) F_3(d) \tag{10}$$

In Equation (10), F_1 (S_{sun}), F_2 (T) and F_3 (d) are empirical variables quantifying the effects of solar radiation, temperature and water vapour deficit on stomatal openness (Jarvis, 1976; Jones, 1983; Lhomme *et al*., 1998).

The soil water stress factor, potential transpiration rate and root density work together to determine the actual transpiration rate, i.e.

$$T_{\text{r},j} = T_{\text{p}} S_j R_j \tag{11}$$

and

$$S_j = \begin{cases} 0 & \text{if } \theta_j < \theta_{j,\text{p}} \\ \dfrac{(\theta_j - \theta_{j,\text{p}})}{(\theta_{j,\text{f}} - \theta_{j,\text{p}})} & \text{if } \theta_{j,\text{p}} < \theta_j < \theta_{j,\text{f}} \\ 1 & \text{if } \theta_j \geq \theta_{j,\text{f}} \end{cases} \tag{12}$$

where S_j (dimensionless) is the water stress factor for the jth soil layer, T_{p} (m day^{-1}) is the total potential transpiration rate, $T_{r,j}$ (m day^{-1}) is the actual transpiration rate from the jth soil layer, R_j (dimensionless) is the fraction of active root in the jth layer, estimated following Jackson *et al*. (1996), and $\theta_{j,f}$ and $\theta_{j,p}$ are the volumetric water contents at the field capacity and the permanent wilting point respectively, which are estimated following Saxton *et al*. (1986) and Letts *et al*. (2000) with the water potential set as 10 kPa at the field capacity and 1500 kPa at the permanent wilting point (Potter *et al*., 1993).

The equation to estimate evaporation is similar to that used to estimate transpiration from the canopy:

$$E_{\text{soil}} = \frac{\Delta(R_{\text{n}} - R_{\text{n}}^{\text{veg}} - G) + \dfrac{\rho C_p d}{r_{\text{a}}}}{L\left[\Delta + \gamma\left(1 + \dfrac{r_{\text{soil}}}{r_{\text{a}}}\right)\right]} \tau_{\text{day}} \tag{13}$$

where G and r_{soil} are the ground heat flux and the ground surface resistance respectively. When snow completely covers the ground surface, r_{soil} is set to zero. Otherwise, the resistance of the ground surface r_{soil} is taken as a function of soil water potential in the first soil layer (Zierl, 2001).

Soil temperature and freeze–thaw cycle

An empirical equation of Yin and App (1993) is employed to convert the mean air temperature T_{a} to the temperature at the ground surface. The vertical distribution of soil temperature is calculated based on the assumption of harmonic variation of temperature around an annual mean with time (Monteith and Unsworth, 1990).

The freeze–thaw process is important in modelling soil moisture dynamics in cold regions (Waelbroeck, 1993). With the assumption that soil water freezes–thaws continuously and uniformly in the range of temperature from −1 to 0 °C (Frolking and Crill, 1994), the fraction of frozen water is estimated as

$$F_{\text{ice}} = \frac{T_{\text{liq}} - T(z, t)}{T_{\text{liq}} - T_{\text{sol}}} \tag{14}$$

where F_{ice} is the fraction of frozen water, T_{liq} is the temperature at which all soil water is liquid (0 °C), T_{sol} is the temperature at which all soil water is frozen (−1·0 °C), and $T(z, t)$ (°C) is the calculated soil temperature.

INITIALIZATION OF WATER TABLE DEPTH AND SOIL C POOLS

In this study, the simulation was carried out in the period from 1901 to 1998 limited by climate data availability. It is necessary to initialize the water table and the various C pools before simulation for the whole period. Their initializations are described here.

Based on the TOMODEL idea, the initial water table of each pixel within a polygon is determined spatially in terms of the spatial distribution of the wetness index, saturated transmissivity, and the long-term polygon mean water table (Beven and Kirkby, 1979; Sivapalan *et al*., 1987). A map of initial water table is produced and input to the model. At each step of the model run, the water table is updated based on simulated soil moisture (Letts *et al*., 2000). The initial polygon mean water table $\overline{Z_{\text{init}}}$ is determined as

$$\overline{Z_{\text{init}}} = \frac{1}{A}\sum_{i=1}^{N}\overline{Z_{\text{init},i}}A_i \tag{15}$$

where N is the number of sub-polygon areas (components) in a polygon, A is the area of the whole polygon, A_i is the area of the ith component, and $\overline{Z_{\text{init},i}}$ is the long-term mean water table of the ith SLC component of a polygon. The value of $\overline{Z_{\text{init},i}}$ is assigned in terms of such attributes as drainage class and slope gradient in the SLC database (Table II).

Two different methods were employed to initialize the size of each C pool. For all C pools of upland sites, the initialization is based on the assumption that C dynamics was approximately in equilibrium prior to 1901 (forest stands younger than 98 years) or the last fire disturbance (forest stands older than 98 years) before industrialization (Chen *et al*., 2003). The simulation is run until C dynamics arrive at quasi-equilibrium (absolute value of Net Ecosystem Productivity (NEP) is smaller than 2% of NPP) using the average of climate data over 1901 to 1910 to drive the model. In simulation, stand-destroying forest disturbance is assumed to occur at a 250 year interval. This interval is roughly equivalent to the mean age of natural mortality and the average fire return period of boreal forests (White *et al*., 2000).

The initialization of C pools of wetland forests is conducted in a different way, since many studies have shown that northern wetlands have never been in equilibrium and continuously act as a persistent sink for CO_2, with an average C accumulation of 0·02–0·03 kg m^{-2} year^{-1} over the past 5000–1000 years (Gorham, 1995). With the assumption that the four biomass pools (foliage, stem, fine root, and coarse root), the five litter pools (surface structural, surface metabolic, soil structural, soil metabolic, and woody), and the two microbial pools (surface microbial and soil microbial) are in steady state in periods prior to 1901 (input equal to output), the initial size of these pools can be determined by solving a set of differential equations regarding the C balance of these pools. The sizes of the slow and passive soil C pools increase continuously (Rapalee *et al*., 1998; Frolking *et al*., 2001). The initial values of these two pools are set following Frolking *et al.* (2001, 2002), with integration ages from 0 to 100 for the slow pool and from 0 to 8000 for the passive pool.

The assumption that the C dynamics were in equilibrium prior to industrialization (1901) or last disturbance before 1901 could result in some errors in the initial values of C pools. However, it is impossible to trace the historical trend of C dynamics for each pixel because of the shortage of historical climate, vegetation and soil

Table II. The initial water table position based on drainage class and slope[a]

Drainage class	Average slope gradient (%)	Defined water table depth (cm)
Very poor	<5	10
	≥5	15
Poor	<10	20
	≥10	30
Imperfect	<15	40
	≥15	50
Moderately well	<15	60
	≥15	70
Well	<15	80
	≥15	100
Rapid	<15	120
	≥15	140
Excessive	<30	150
	≥30	200

[a] The definition of drainage class and slope is based on that in the SLC database. Combined with other attributes, this information is used to set the initial water table depth (http://sis.agr.gc.ca/cansis/nsdb/slc/v2·0/component/drain.html).

C inventory data. One possible solution to this problem is to run the model using mean climate, N deposition and stand age for a long time to reach a near-equilibrium state in the environment before industrialization. The error related to the initialization would be significantly reduced after a 98 year simulation from 1901 to 1998 (Chen *et al*., 2003).

DATA USED

A variety of data sets, including remote sensing, climate, soil texture, N deposition, and digital elevation maps (DEMs), were produced and compiled from various sources to drive the model. All spatial data were made compatible with remote-sensing imagery in a 1 km resolution grid of 5700 × 4800 pixels. All grids are in a standard Lambert conformal conic (LCC) projection with 49 and 77 °N standard parallels and a 95 °W meridian. The spatially distributed data sets used in the simulation are listed in Table III.

RESULTS AND DISCUSSION

Comparison of simulated soil organic C with SLC

For model calibration and validation, the polygon-mean C stock values were compiled from attributes such as soil bulk density, depth, C content of various soil layers, and the area of each component in the SLC database. In total, there are about 15 000 SLC polygons in the SLC. Each polygon contains several components, with respective attributes defined. There are about 32 000 SLC components. Only 10 040 SLC components have soil C stock values measured at representative or sample sites. The 2228 polygons used in the analysis are those having components with soil C measurements accounting for over 50% of the area in the whole polygon. Firstly, half of these polygons were uniformly randomly sampled for model calibration and the remaining polygons were used to validate the model. Modelled soil C stocks were compared against SLC data for both calibration and validation data sets (Figure 2). The root-mean-square error (RMSE) values for C are 16·83 kg m^{-2} and 24·97 kg m^{-2} for the calibration set and validation set respectively. The model underestimations for the validation data set are even smaller than those for the calibration data set. The values of mean biased error (MBE) for C equal −1·98 kg m^{-2} for the validation

Table III. Data sets used in the simulation

Data set	Source	Reference
LAI map in 1994	Remote sensing	Chen *et al.* (2002)
Landcover in 1995	Remote sensing	Cihlar *et al.* (1998)
Sand age map in 1998	Big forest fire data set, forest inventory and remote sensing	Chen *et al.* (2003)
Annual NPP in 1994	Output from BEPS	Liu *et al.* (1999, 2002)
Monthly mean air temperature	Interpolated from the data of UK Climate Research Unit	New *et al.* (1999, 2000), Liu *et al.* (1999)
Monthly precipitation	Interpolated from the data of UK Climate Research Unit	New *et al.* (1999, 2000), Liu *et al.* (1999)
Monthly solar radiation	Simulated using air temperature range, precipitation and relative humidity	Thornton and Running (1999)
Annual N deposition in 1984	Interpolated and extrapolated using measurements at stations	Ro *et al.* (1995), Chen *et al.* (2003)
Soil texture and soil organic C	Complied from SLC database	Shields *et al.* (1991), Schut *et al.* (1994), Tarnocai (1996), Lacelle (1998)
Wetness index	Derived from Canada 3D 30	Beven and Kirkby (1979), Beven (1997)

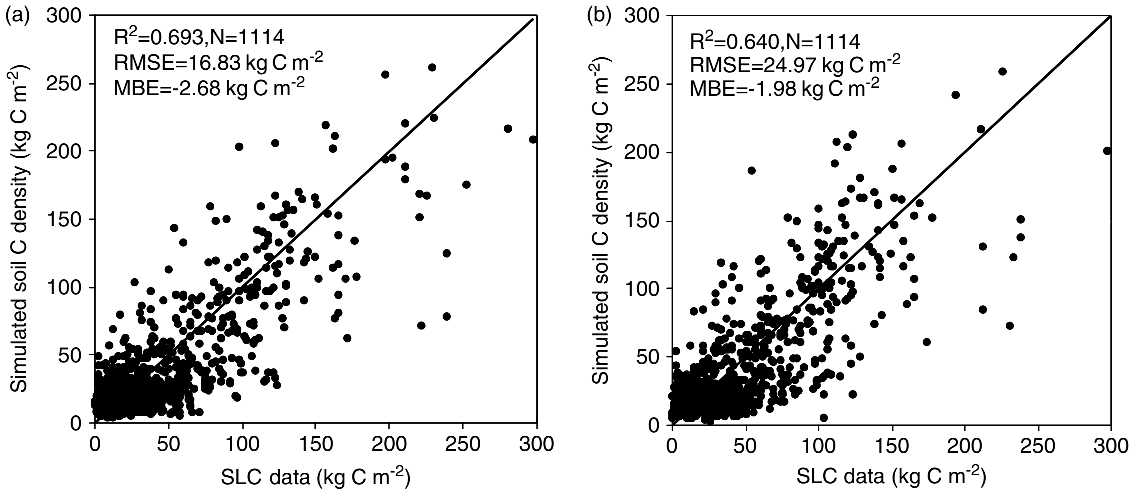

Figure 2. Comparison of total soil C stocks modelled using InTEC V 3·0 with data from the SLC: (a) for model calibration; (b) for model validation

set and $-2{\cdot}68$ kg m^{-2} for the calibration set. The model captures a slightly smaller degree of the spatial variation of soil C in the validation data set ($R^2 = 0{\cdot}640$, $N = 1114$) compared with the calibration data set ($R^2 = 0{\cdot}693$, $N = 1114$).

A comparison of InTEC V3·0 and InTEC V2·0 using 2228 SLC polygons was conducted. Compared with InTEC 2·0, InTEC V3·0 improves the simulation of soil C stocks (Figure 3). For InTEC V2·0, the MBE of simulated soil C stocks is $-17{\cdot}05$ kg m^{-2}, mainly resulting from the underestimations of soil C in poorly drained wetland polygons located around Hudson Bay and the Mackenzie Valley lowlands. In such regions, the magnitude of the C underestimation can be even larger than 60 kg m^{-2}. For InTEC V3·0, although the underestimation of soil C in poorly drained wetland polygons still exists, the magnitude of the MBE value for C decreased from 17·05 to 2·33 kg m^{-2}, and the RMSE decreased from 40·39 to 24·58 kg m^{-2}, demonstrating that InTEC V3·0 has substantially improved over InTEC V2·0 for simulating soil C stocks.

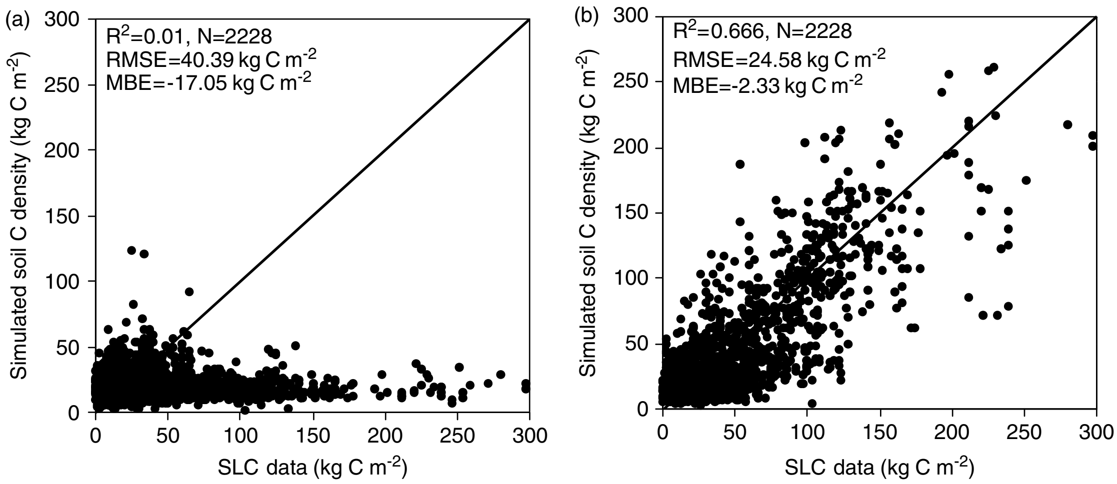

Figure 3. Comparison of modelled total soil C stocks with data from the SLC: (a) from InTEC V2·0; (b) from InTEC V3·0

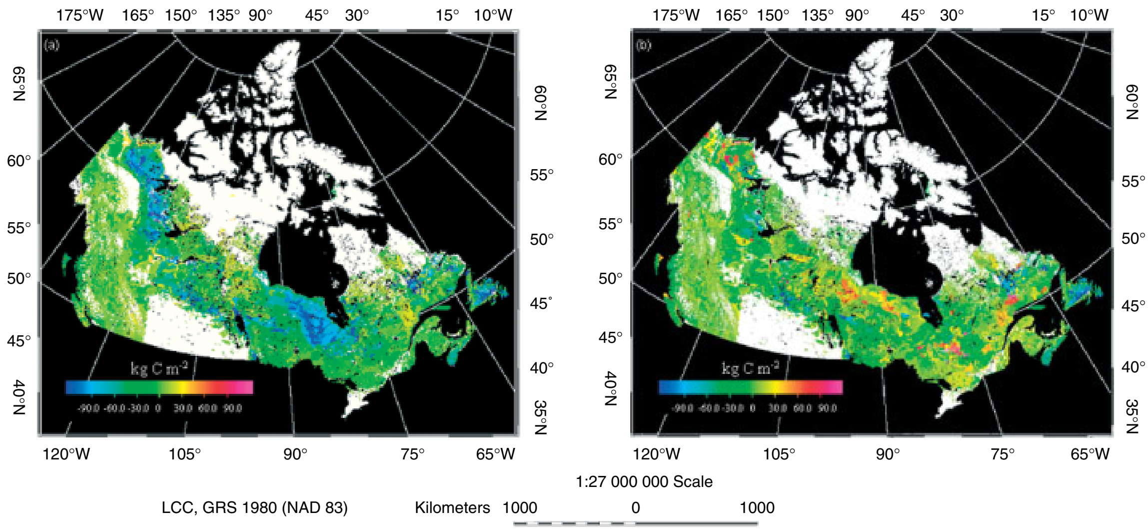

Figure 4. Spatial distribution of the difference between simulated soil C density from InTEC model and SLC data: (a) for InTEC V2·0; (b) for InTEC V3·0. The values in the map are simulated soil C density minus the SLC value. Negative values represent negative model biases and positive values represent positive model biases

To evaluate the Canada-wide model simulation, maps were produced (Figure 4) showing the difference between simulated C for each version of the model and SLC data. In Figure 4, the values equal the simulated soil C density minus the SLC value and demonstrate that InTEC V3·0 effectively alleviated the negative bias in soil C estimation in wetlands by InTEC V2·0. However, the negative bias from InTEC V3·0 still exists in some regions, such as part of the Newfoundland Island (blue coloured areas in Figure 4). Overestimation of soil C also occurs, to a small extent, mainly in the southwest part of Hudson Bay and part of Mackenzie Valley (red and pink coloured areas in Figure 4).

The remaining discrepancy between modelled soil C and SLC data can be attributed to the following reasons. In BEPS and InTEC, LAI, a key variable for NPP calculation, is derived from remote-sensing data. Atmospheric noise can significantly influence the LAI calculation. Although remote-sensing data used in this simulation was carefully processed, it is impossible to remove all atmospheric effects in all regions. The remaining atmospheric noise in remote-sensing data may introduce uncertainty in the calculation of NPP. In these two models, overstory and understory are lumped together. This strategy has the advantage of reducing computation and avoiding the numerical separation between overstory and understory, which is difficult for large areas. However, it has the possibility of underestimating the contribution of the understory to soil C accumulation. The exclusion of the moss layer in poorly drained regions may also give rise to errors in soil C simulation (Frolking *et al*., 2002). The values of model parameters were determined based on published results and available data sets. Some parameters, such as allocation coefficients of NPP to biomass C pools, the turnover rates of foliage and fine root C pools, are assumed to be spatially and temporally constant for the same forest types. This assumption may not always be realistic. The horizontal redistribution in this model is simulated using the TOPMODEL approach with the assumption that the water table varies in parallel with the surface topography. This approach is possibly not effective on the boreal plains in the provinces of Albert and Ontario, where the bedrock plays an important role in water table spatial variations. The effect of this assumption in simulating soil moisture and water table is, to some extent, controlled through the use of drainage class, allowing for marked improvement in soil C simulations in lowland areas.

Comparison of modelled biomass with forest inventory data

Forest biomass is the source of soil C, and the accuracy in the simulated soil C distribution depends greatly on the biomass distribution. Forest biomass in each pixel is calculated as the sum of C in stems, roots and foliage. The total C accumulation of vegetation depends on the NPP, coefficients of C allocation to the various vegetation pools, and turnover rates of these pools. The use of forest inventory of above-ground biomass allows us to check the reliability of NPP allocation coefficients. The simulated Canada-wide aboveground biomass (C) is in a range from 1·0 kg m^{-2} to 9·0 kg m^{-2}, increasing from subarctic to moderate temperate regions. These values fall in the range of inventory data and are also similar to the results simulated at the global scale by Kucharik *et al*. (2000). The spatial distribution pattern is very similar to that of NPP (Liu *et al*., 2002). Spatially, the simulated result and inventory data are in good agreement for most areas, with the exception in the moderate temperate and southern part of Pacific cordilleran regions (Figure 5). In the moderate temperate region, where deciduous forests dominate, the model result is 20 to 30% larger than the inventory data. In contrast to this case, in southern Pacific cordilleran regions, where land cover is a mixture of forests, the simulated above-ground biomass is only roughly half of the value of inventory data. Figure 6 shows a comparison of the modelled C in above-ground biomass with the forest inventory data on the basis of forest type. Modelled above-ground biomass values for mixed and deciduous forest types are about 30% larger than the inventory data. This may indicate that the allocation coefficients of NPP to the above-ground biomass pools are too large, although the coefficients we used are within one standard deviation of the ground measurement at an aspen site (Gower *et al*., 1997). The modelled values of above-ground biomass in sparse forests are considerably smaller than those in the inventory, but the inventory data for this cover type are insufficient and, therefore, may not be reliable. The best agreement between modelled and inventory data was obtained for conifer forests, which occupy about 53% of Canada's forested areas. Inaccuracies in above-ground biomass estimation have importance in soil C stock estimation. Clearly, significant improvements can still be made in the relative allocations to above-ground and below-ground biomass components once more field data become available.

Soil C accumulation rate

Simulated temporal variations of Canada-wide average C in vegetation, soil and the ecosystem are summarized in Figure 7. The nationwide C accumulation rate of forests and wetlands was 0·021 kg m^{-2} $year^{-1}$ when averaged over the period from 1901 to 1998, with contributions of 0·011 kg m^{-2} $year^{-1}$ and 0·01 kg m^{-2} $year^{-1}$ from vegetation and soil respectively. The combined effects of fire disturbance, climate and atmospheric changes have resulted in net increases in C in both soil and vegetation. At the early

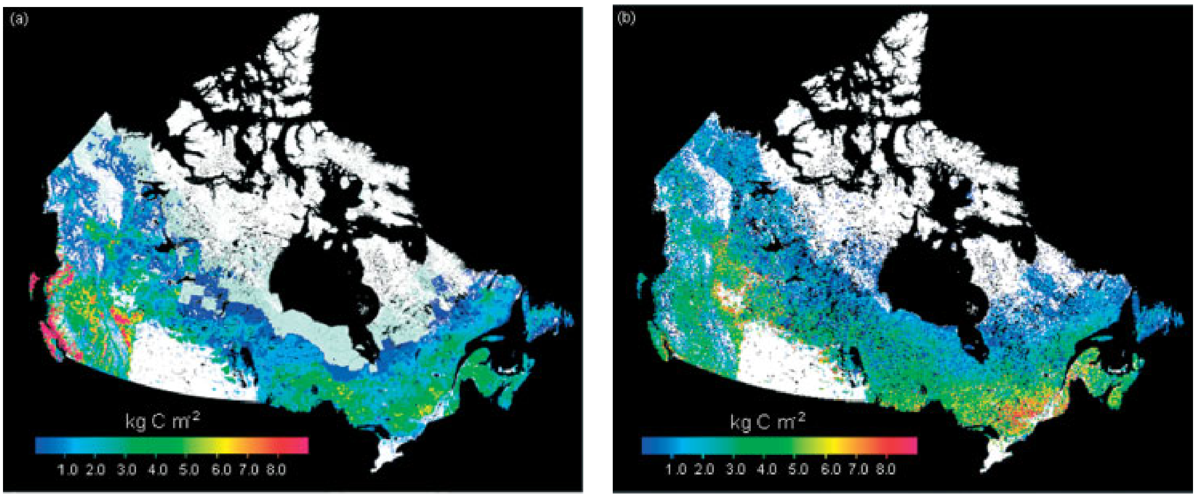

Figure 5. Spatial distribution of simulated above-ground biomass against inventory data: (a) inventory data; (b) model results

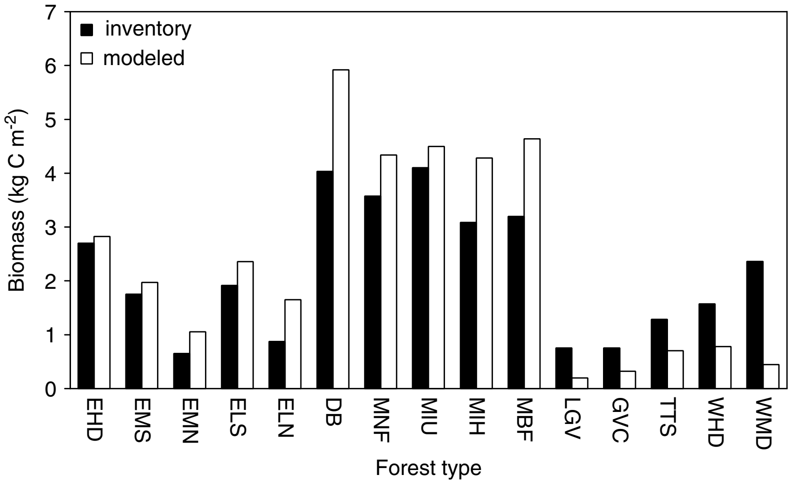

Figure 6. Comparison of modelled above-ground biomass with data from forest inventory by forest type. Forest classification: EHD, high density evergreen needleleaf forest; EMS, medium density southern evergreen forest; EMN, medium density northern evergreen forest; ELS, low density southern evergreen forest; ELN, low density northern evergreen forest; DB, deciduous broadleaf forest; MNF, mixed needleleaf forest; MIU, mixed intermediate uniform forest; MIH mixed intermediate heterogeneous forest; MBF, mixed broadleaf forest; LGV, low green vegetation cover; GVC, green vegetation cover; TTS, transition treed shrubland; WHB, high density wetland/shrubland; WMB, medium density wetland/shrubland

20^{th} century, vegetation C decreased due to intensive fire disturbance. Vegetation C began to increase steadily from around 1915, due to the combined positive effects of increased temperature, CO_2 fertilization and N deposition on NPP. This trend continued until the late 1970s. Since then, vegetation C has fluctuated due to dramatic increases in the frequency and magnitude of fire disturbance. The change of soil C lagged that of vegetation C by about 15 years because of the slow litter transfer from biomass to soil. In contrast to vegetation C, in years with large burned areas, soil C increased dramatically under the assumption that fire disturbance transferred all root C and 75% woody C into soil. Then it decreased until the forest regrowth produced enough litter to offset the loss from heterotrophic respiration. The amplitude of soil C

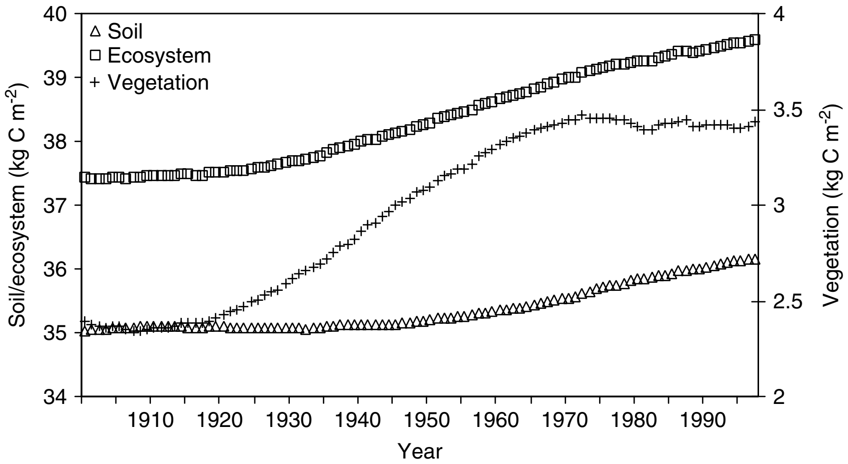

Figure 7. Simulated temporal variation of the average C density in vegetation, soil and ecosystem. The ecosystem C is the sum of both vegetation C and soil C. The increase of C density is larger in vegetation than in soil

accumulation was smoothed by the adjustment of enhanced soil respiration resulting from increased soil temperature. The Canada-wide average accumulation rate of soil C from 1900 to 1998 is 0·01 kg m^{-2} $year^{-1}$, which is only 50% of the mean soil C accumulation rate for forest stands older than 13 years in the northern study area (NSA) of the Boreal Ecosystem–Atmosphere Study (BOREAS) reported by Rapalee *et al*. (1998). Their values for C range from −0·021 to 0·068 kg m^{-2} $year^{-1}$, with the average equal to 0·02 kg m^{-2} $year^{-1}$.

The soil C accumulation rate from InTEC V3·0 varies spatially from about −0·02 kg m^{-2} $year^{-1}$ (net loss) in recently burned areas to over 0·03 kg m^{-2} $year^{-1}$ (net accumulation) in regions such as the wetlands on the margins of Hudson Bay and the southern parts of the provinces of Ontario and Quebec. The southern forests of these two provinces are dominantly deciduous and at productive ages. Relatively high N deposition here also increases the productivity of forests. These factors allow soils to accumulate C at high rates. The C accumulation rates are generally less than 0·010 kg m^{-2} $year^{-1}$ in most Mackenzie Valley regions due to very low NPP values (Liu *et al*., 2002). The simulated average accumulation rate of soil C and its dependence on stand age and drainage classes are within the range of published values. Trumbore and Harden (1997) indicated that, in the NSA of BOREAS, the accumulation rate of soil C depends on stand age and drainage class, ranging from close to zero for sandy soils in jack pine stands, to 0·003–0·01 kg m^{-2} $year^{-1}$ for moderately to poorly drained sites in mature forest stands, to 0·03 kg m^{-2} $year^{-1}$ for a productive fen. Rapalee *et al*. (1998) supported this conclusion and also pointed out that the accumulation rate of soil C is inversely related to stand age over 13 years old in all drainage classes. Poorly drained sites accumulate soil C quicker than very poorly drained sites. Frolking *et al*. (2001) estimated that, in the past 8000 years, the mean accumulation rates of C are 0·022 kg m^{-2} $year^{-1}$ for fens and 0·036 kg m^{-2} $year^{-1}$ for bogs in eastern Canada. However, they currently accumulate C at the rates of 0·006 kg m^{-2} $year^{-1}$ and 0·020 kg m^{-2} $year^{-1}$ respectively.

SUMMARY

The pixel-based InTEC model has been improved after modifications, i.e. new model parameterizations and the development of a hydrological submodel, which simulates the spatial and temporal dynamics of soil temperature and moisture within three soil layers using spatially distributed climate, vegetation, soil, DEMs and drainage class data. This TOPMODEL-based quasi-three-dimensional hydrological submodel can capture the mechanisms controlling both vertical and lateral redistributions of soil water in heterogeneous areas, as well as of other components of the water and energy balance. It is able to simulate the spatial distribution pattern of soil moisture under different topographic conditions, which makes it possible to simulate the influence of hydrological processes on productivity, decomposition and accumulation rates of soil C with some confidence at the regional scale. The modification of a comprehensive below-ground biogeochemical submodel allows for an elaborate description of below-ground biochemical processes in various drainage classes. InTEC V3·0 is now capable of simulating the combined effects of biophysical and biogeochemical processes on the spatial distribution of the C balance at the regional scale with a relatively high spatial resolution (1 km). This improved model may be one of few C simulation models suitable for both upland and wetland forests at regional scales.

Several sets of measurements, including drainage class, soil C density, soil physical properties available in the SLC database, and above-ground biomass from forest inventory, were employed to run the model and to validate some of the results. Compared with soil C data available in the SLC on the basis of polygons, the modified pixel-based InTEC V3·0 can capture the major spatial variation of soil C stocks (66·6%). The major improvement was achieved in the simulation of C stocks in forested and non-forested wetlands, for which negative biases in simulated soil C stocks were greatly reduced. The model captures 80% of the variance in the nationwide mean of above-ground biomass among 15 forest cover types. For conifer forests, which occupy about 53% of Canada's forested areas, the discrepancy in above-ground biomass (C) between the model and the forest inventory is less than 0·4 kg m^{-2}.

However, several problems still exist in this study. From this current model, the overestimation of soil C stocks for some wetlands is still noticeable and needs further studies to develop more precise descriptions of the hydrological, biogeochemical and biophysical processes. For example, vegetation composition, historical NPP, and drainage classes are all important for simulating soil C accumulation rates and the size of the soil C stock. The simplification of a unique cover type and one vegetation layer within a 1 km $\times$ 1 km pixel cannot completely describe the processes of C cycles in the atmosphere, vegetation and soil system. In northern wetlands, several vegetation types usually coexist in a pixel in coarse-resolution images, and understory vegetation can contribute considerable amounts of C to the soil organic matter. For example, mosses are critical in soil C simulation for peatlands. The mechanism by which vegetation with different rooting depths influences the decomposition rate of soil C has not yet been included in the model. The same values of chemical properties of vegetation influencing the decomposition rate, such as lignin and N contents, are assigned to each of several major cover types without vegetation composition considered. The above shortcomings of this current model may induce uncertainties in soil C simulation. Other factors contributing to errors in simulating soil C stocks in some regions are the spatial and temporal resolutions of the model. In particular, the 1 km $\times$ 1 km spatial resolution image, which smoothes local topography and, consequently, the redistribution of soil water, induces some errors in simulation. These problems can be overcome, to some extent, with higher resolution data used and/or scaling parameters calibrated based on more field measurements.

ACKNOWLEDGEMENTS

We would like to thank Dr Josef Cihlar of the Canada Centre for Remote Sensing for the use of the Canada-wide landc over map, Dr Dave Price and Dr Brian Amiro of the Canadian Forest Service for the forest inventory and large fire polygon data sets, and Agriculture and Food Canada for the Soil Landscape of Canada. Individuals who provided helpful comments to this work include Professor Ferko Cscillag, Professor Bill Gough, and Professor Brian Branfireun of the University of Toronto. We also gratefully acknowledge the constructive comments by two anonymous reviewers and the Guest Co-Editor, which helped improve the quality of manuscript greatly.

REFERENCES

Abramopoulos F, Rosenzweig C, Choudhury B. 1988. Improved ground hydrology calculation for global climate models (GCMs): soil water movement and evapotranspiration. *Journal of Climate* **1**: 921–941.

Arnold JG, Williams JR. 1995. SWRRB—a watershed scale model for soil and water resources management. In *Computer Models of Watersheld Hydrology*, Singh VP (ed.). Water Resources Publications: Highlands Ranch, CO; 847–908.

Bhatti JS, Apps MJ, Tarnocai C. 2002. Estimates of soil organic carbon stocks in central Canada using three different approaches. *Canadian Journal of Forest Research* **32**: 805–812.

Beven K. 1997. TOPMODEL: a critique. *Hydrological Processes* **11**: 1069–1085.

Beven KJ, Kirkby MJ. 1979. A physically based variable contributing model of basin hydrology. *Hydrological Sciences Bulletin* **24**: 43–69.

Campbell GS, Norman JM. 1998. *An Introduction to Environmental Biophysics*. Springer: New York.

Chen JM, Liu J, Cihalr J, Goulden ML. 1999. Daily canopy photosynthesis model through temporal and spatial scaling for remote sensing applications. *Ecological Modelling* **124**: 99–119.

Chen JM, Pavlic G, Brown L, Cihlar J, Leblance SG, White HP, Hall RJ, Peddle DR, King DJ, Trofymow JA, Swift E, Sanden VD, Pellikka PKE. 2002. Derivation and validation of Canada-wide coarse-resolution satellite imagery and ground measurements. *Remote Sensing of Environment* **80**: 165–184.

Chen JM, Ju W, Cihlar J, Price D, Liu J, Chen WJ, Pan JJ, Black A, Barr A. 2003. Spatial distribution of C sources and sinks in Canada's forests based on remote sensing. *Tellus Series B: Chemical and Physical Meteorology* **55**: 622–641.

Chen W, Chen J, Cihlar J. 2000a. An integrated terrestrial ecosystem C-budget model based on changes in disturbance, climate, and atmospheric chemistry. *Ecological Modelling* **135**: 55–79.

Chen WJ, Chen JM, Liu J, Cihlar J. 2000b. Approach for reducing uncertainties in regional forest carbon balance. *Global Biogeochemical Cycles* **14**(3): 839–850.

Cihlar J, Xiao Q, Chen JM, Beaubien J, Fung K, Latifovic R. 1998. Classification by progressive generalization: a new automated methodology for remote sensing multichannel data. *International Journal of Remote Sensing* **19**: 2685–2704.

Dickson RE, Sellers AH, Kennedy PJ, Wilson MF. 1986. *Biosphere–atmosphere transfer scheme (BATS) for the NCAR community climate model*. NCAR Technical Note TN-275, National Center for Atmosphere Research, Boulder, CO, USA.

Farquhar GD, von Caemmerer S, Berry JA. 1980. A biochemical model of photosynthetic CO_2 assimilation in leaves of C_3 species. *Planta* **149**: 78–90.

Friend AD, Stevens AK, Knox RG, Cannell MGR. 1997. A process-based, terrestrial biosphere model of ecosystem dynamics (Hybrid V3·0). *Ecological Modelling* **95**: 249–287.

Frolking SE, Crill P. 1994. Climate controls on temporal variability of methane flux from a poor fen in southeastern New Hampshire: measurement and modeling. *Global Biogeochemical Cycles* **8**(4): 385–397.

Frolking SE, Bubier JL, Moore TR, Ball T, Bellisario LM, Bhardwaj A, Caroll P, Crill PM, Lafleur PM, McCaughey JH, Roulet NT, Suyker AE, Verma SB, Waddington JM, Whiting GJ. 1998. Relationship between ecosystem productivity and photosysnthetically active radiation for northern peatlands. *Global Biogeochemical Cycles* **12**(1): 115–126.

Frolking SE, Roulet NT, Moore TR, Richard PJH, Lavoie M, Muller SD. 2001. Modeling northern peatland decomposition and peat accumulation. *Ecosystem* **4**: 479–498.

Frolking SE, Roulet NT, Moore TR, Lafleur PM, Bubier JL, Crill PM. 2002. Modeling the seasonal to annual C balance of Mer Bleue bog, Ontario, Canada. *Global Biogeochemical Cycles* **16**(3): DOI: 10·1029/2001GB001457.

Gorham E. 1995. The biogeochemistry of northern peatlands and its possible response to global warming. In *Biotic Feedbacks in the Global Climatic System: Will the Warming Feed the Warming?*, Woodwell GM, Mackenzie FT (eds). Oxford University Press: New York; 169–187.

Gough WA, Wolfe E. 2001. Climate change scenarios for Hudson Bay, Canada, from general circulation models. *Arctic* **54**: 142–148.

Gower ST, Vogel JG, Norman JM, Kucharik CJ, Steele SJ, Stow TK. 1997. Carbon distribution and aboveground net primary production in aspen, jack pine, and black spruce in Saskatchewan and Manitoba Canada. *Journal of Geophysical Research* **102**(D24): 29 029–29 042.

Griend AAVD. 1993. On the relationship between thermal emissivity and normalized difference vegetation index for natural surfaces. *International Journal of Remote Sensing* **14**(6): 1119–1131.

Gurney KR, Law RM, Denning AS, Rayner PJ, Baker D, Bousquest P, Bruhwilder L, Chen YH. 2002. Towards robust regional estimates of CO_2 sources and sinks using atmospheric transport models. *Nature* **415**: 626–630.

Haxeltine A, Prentice IC. 1996. Biome3: an equilibrium terrestrial biosphere model based on ecophysiological constraints, resource availability, and competition among function types. *Global Biogeochemical Cycles* **10**(4): 693–709.

Houghton RA. 1999. The annual net flux of C to the atmosphere form changes in land use 1850–1990. *Tellus Series B: Chemical and Physical Meteorology* **51**: 298–313.

Jackson RB, Canadell J, Ehleringer JR. 1996. A global analysis of root distributions for terrestrial biomes. *Oecologia* **108**: 389–411.

Jarvis PG. 1976. The interpretation of the variations in leaf water potential and stomatal conductance found in canopies in the field. *Phiolosophical Transactions of the Royal Society of London, Series B: Biological Sciences* **273**: 593–610.

Jones HG. 1983. *Plants and Microclimate*. Cambridge University Press: New York..

Kergoat L. 1998. A model for hydrological equilibrium of leaf area index on a global scale. *Journal of Hydrology* **212–213**: 268–286.

Kucharik CJ, Foly JA, Delire C, Fisher VA, Coe MT, Lenters JD, Yong-Molling C, Ramankutty N. 2000. Testing the performance of a dynamic global ecosystem model: water balance, C balance, and vegetation structure. *Global Biogeochemical Cycles* **14**(3): 795–825.

Lacelle B. 1998. Canada's soil organic carbon database. In *Soil Processes and the Carbon Cycle*, Lal R, Kimbla J, Follett RF, Stewart BA (eds). CRC Press: Boca Raton; 93–102.

Letts MG, Roulet NT, Comer NT, Skarupa MR, Verseghy D. 2000. Parameterization of peatland hydraulic properties for the Canadian land surface scheme. *Atmosphere–Oceans* **38**: 141–160.

Lhomme JP, Elguero E, Chehbouni A, Boulet G. 1998. Stomatal control of transpiration: examination of Monteith's formulation of canopy resistance. *Water Resources Research* **34**(9): 2301–2308.

Liu J, Chen JM, Cihlar J, Chen W. 1999. Net primary productivity distribution in the BOREAS study region from a process model driven by satellite and surface data. *Journal of Geophysical Research* **104**(D22): 27 735–27 754.
Liu J, Chen JM, Cihlar J. 2002. Remote sensing based estimation of net primary productivity over Canadian landmass. *Global Ecology and Biogeography* **11**: 115–129.
Lloyd J, Taylor JA. 1994. On the temperature dependence of soil respiration. *Functional Ecology* **8**: 315–323.
McGuire AD, Melillo JM, Joyce LA, Kicklighter DW, Grace AL, Moore III B, Vörösmarty CJ. 1992. Interaction between carbon and nitrogen dynamics in estimating net primary production for potential vegetation in North America. *Global Biogeochemical Cycles* **6**(2): 101–124.
Monteith JL, Unsworth MH. 1990. *Principles of Environmental Physics*. Edward Arnold: London.
Neilson RP. 1995. A model predicting continental-scale vegetation distribution and water balance. *Ecological Applications* **5**(2): 362–385.
Neilson RP, Marks D. 1994. A global perspective of regional vegetation and hydrologic sensitivities from climate change. *Journal of Vegetation Science* **5**: 715–730.
New MG, Hulme M, Jones PD. 1999. Representing 20th century space–time climate variability. I: development of a 1961–1990 mean monthly terrestrial climatology. *Journal of Climate* **12**: 829–856.
New MG, Hulme M, Jones PD. 2000. Representing 20th century space–time climate variability. II: development of 1901–1996 monthly terrestrial climate fields. *Journal of Climate* **13**: 2217–2238.
Parton WJ, Schimel DS, Cole CV, Ojima DS. 1987. Analysis of factors controlling soil organic matter levels in Great Plains grasslands. *Soil Science Society of America Journal* **51**: 1173–1179.
Parton WJ, Scurlock JM, Ojima DS, Gilmanov TG, Scholes RJ, Schimel DS, Kirchner T, Menaut J-C, Seastedt T, Moya EG, Kamnalrut A, Kinyamario JI. 1993. Observation and modeling of biomass and soil organic matter dynamics for the grassland and biome worldwide. *Global Biogeochemical Cycles* **7**(4): 785–809.
Potter CS. 1997. An ecosystem simulation model for methane production and emission for wetlands. *Global Biogeochemical Cycles* **11**(4): 495–506.
Potter CS. 1999. Terrestrial biomass and the effects of deforestation on the global C cycle. *Bioscience* **49**(10): 769–778.
Potter CS, Klooster ST. 1998. Interannual variability in soil trace gas (CO_2, N_2O, NO) fluxes and analysis of controllers on regional to global scales. *Global Biogeochemical Cycles* **12**(4): 621–635.
Potter CS, Randerson JT, Field CB, Matson PA. 1993. Terrestrial ecosystem production: a process model based on global satellite and surface data. *Global Biogeochemical Cycles* **7**(4): 811–841.
Potter CS, Bubier J, Crill P, Lafleur P. 2001. Ecosystem modeling of methane and carbon dioxide flues for boreal forest sites. *Canadian Journal of Forest Research* **31**: 208–223.
Raich JW, Rastetter EB, Melillio JM, Kicklighter DW, Steudler PA, Peterson BJ, Grace AL, Moore III B, Vörösmarty CJ. 1991. Potential net primary production in South America: application of a global model. *Ecological Application* **1**(4): 399–429.
Rapalee G, Trumbore SE, Davidson EA, Harden JW, Veldhuis H. 1998. Soil C stocks and their rates of accumulation and loss in a boreal landscape. *Global Biogeochemical Cycles* **12**(4): 687–701.
Ro C, Vet R, Ord D, Holloway A. 1995. *National Atmospheric Chemistry Database 1993 annual report, acid precipitation in eastern Northern America*. Atmospheric Environment Service, Environment Canada.
Roulet NT, Munro DS, Mortsch L. 1997. Wetlands. In *The Surface Climates of Canada*, Baily WG, Oke TR, Rouse WR (eds). McGill-Queen's University Press: Montreal; 149–171.
Running SW, Gower ST. 1991. Forest-BGC, a general model if forest ecosystem processes for regional applications, II, dynamic allocation and nitrogen budgets. *Tree Physiology* **9**: 147–160.
Satterlund DR. 1979. An improved equation for estimating long-wave radiation from the atmosphere. *Water Resources Research* **15**: 1649–1650.
Saxton KE, Rawls WJ, Romberger JS, Papendick RI. 1986. Estimating generalized soil-water characteristics from texture. *Soil Science Society of America Journal* **50**: 1031–1036.
Schimel DS, House JI, Hibbard KA, Bousquet P, Cialis P, Peylin P, Braswell BH, Apps MJ, Baker D, Bondeau A, Canadell J, Churkina G, Cramer W, Denning AS, Field CB, Friedlingstein P, Goodale C, Heimann M, Houghton RA, Melillo JM, Moore III B, Murdiyarso D, Noble I, Pacala SW, Prentice IC, Raupach MR, Rayer PJ, Scholes RJ, Steffen WL, Wirth C. 2001. Recent patterns and mechanisms of C exchange by terrestrial ecosystems. *Nature* **414**: 169–172.
Schut P, Shields J, Tarnocai C, Coote D, Marshall I. 1994. Soil Landscapes of Canada—an environmental reporting tool. In *Canadian Conference on GIS Proceedings*, 6–10 June, Ottawa; 953–965.
Sellers PJ, Mintz Y, Yud YC, Dalcher A. 1986. A simple biosphere model (SiB) for use within general circulation models. *Journal of the Atmospheric Sciences* **43**(6): 505–531.
Sellers PJ, Randall DA, Collatz GJ, Berry JA, Field CB, Dazlich DA, Zhang C, Bounoua L. 1996. A revised land surface parameterization (SiB2) for atmospheric GCMs. part I: model formulation. *Journal of Climate* **9**: 676–705.
Shields JA, Tarnocai C, Valentine KWG, MacDonald KB. 1991. *Soil Landscapes of Canada, Procedures Manual and User's Handbook. Land Resource Research Center, Agricultural Canada Publication* 1868/E. Agricultural Canada: Ottawa, Ontario.
Sivapalan M, Beven K, Wood EF. 1987. On hydrologic similarity, 2. A scaled model of storm runoff production. *Water Resources Research* **23**(12): 2266–2278.
Stieglitz M, Rind D, Famiglietti J, Rosenzweig C. 1997. An efficient approach to modeling the topographic control of surface hydrology for regional and global climate modeling. *Journal of Climate* **10**: 118–137.
Tarnocai C. 1998. The amount of organic carbon in various soil orders and ecological provinces in Canada. In *Soil Processes and the Carbon Cycle*, Lal R, Kimbla J, Follett RF, Stewart BA (eds). CRC Press: Boca Raton; 81–92.
Thornton PE, Running SW. 1999. An improved algorithm for estimating incident daily solar radiation from measurements of temperature, humidity, and precipitation. *Agricultural and Forest Meteorology* **93**: 211–228.

Tolonen K, Vasander H, Damman AWH, Clymo RS. 1992. Preliminary estimate of long-term C accumulation and loss in 25 boreal peatlands. *Suo* **43**: 277–280.

Trumbore SE, Harden JW. 1997. Accumulation and turn over of C in organic and mineral soils of BOREAS northern study area. *Journal of Geophysical Research* **102**(D4): 28 817–28 830.

Waelbroeck C. 1993. Climate–soil process in the presence of permafrost: a system modelling approach. *Ecological Modelling* **69**: 185–225.

White A, Cannell MGR, Friend AD. 2000. The high-latitude terrestrial carbon sink: a model analysis *Global Change Biology* **6**: 227–245.

Wigmosta MS, Vail LW, Lettenmaier DP. 1994. A distributed hydrological–vegetation model for complex terrain. *Water Resources Research* **30**(6): 1665–1679.

Yin X, App PA. 1993. Predicting forest soil temperature from monthly temperature and precipitation records. *Canadian Journal of Forest Research* **23**: 2521–2536.

Zierl B. 2001. A water balance model to simulate drought in forested ecosystem and its application to the entire forested area in Switzerland. *Journal of Hydrology* **242**: 115–136.

